Title

Photochemical Dearomative Cycloadditions of Quinolines and Alkenes: Scope and Mechanism Studies.

Journal

Journal of the American Chemical Society, 144(38)

Authors

Guo, Renyu
Adak, Souvik
Bellotti, Peter
et al.

Publication Date

2022-09-28

DOI

10.1021/jacs.2c07726

Peer reviewed

HHS Public Access

Author manuscript

J Am Chem Soc. Author manuscript; available in PMC 2023 September 28.

Published in final edited form as:

J Am Chem Soc. 2022 September 28; 144(38): 17680–17691. doi:10.1021/jacs.2c07726.

Photochemical Dearomative Cycloadditions of Quinolines and Alkenes: Scope and Mechanism Studies

Renyu Guo,
Department of Chemistry, Indiana University, Bloomington, Indiana 47405, United States

Souvik Adak,
Department of Chemistry, Indiana University, Bloomington, Indiana 47405, United States

Peter Bellotti,
Organisch-Chemisches Institut, Westfälische Wilhelms-Universität Münster, 48149 Münster, Germany

Xinfeng Gao,
Department of Chemistry, Indiana University, Bloomington, Indiana 47405, United States

W. Walker Smith,
Department of Chemistry, Indiana University, Bloomington, Indiana 47405, United States

Sam Ngan Le,
Department of Chemistry and Biochemistry, Oberlin College, Oberlin, Ohio 44074, United States

Jiajia Ma,
Organisch-Chemisches Institut, Westfälische Wilhelms-Universität Münster, 48149 Münster, Germany

K. N. Houk,
Department of Chemistry and Biochemistry, University of California, Los Angeles, Los Angeles, California 90095, United States

Frank Glorius,
Organisch-Chemisches Institut, Westfälische Wilhelms-Universität Münster, 48149 Münster, Germany

Shuming Chen,

Corresponding Authors: **K. N. Houk** – Department of Chemistry and Biochemistry, University of California, Los Angeles, Los Angeles, California 90095, United States; houk@chem.ucla.edu, **Frank Glorius** – Organisch-Chemisches Institut, Westfälische Wilhelms-Universität Münster, 48149 Münster, Germany; glorius@uni-muenster.de, **Shuming Chen** – Department of Chemistry and Biochemistry, Oberlin College, Oberlin, Ohio 44074, United States; shuming.chen@oberlin.edu, **M. Kevin Brown** – Department of Chemistry, Indiana University, Bloomington, Indiana 47405, United States; brownmkb@indiana.edu.

Supporting Information

The Supporting Information is available free of charge at https://pubs.acs.org/doi/10.1021/jacs.2c07726.
Experimental procedures, analytical data for all new compounds (PDF)

Accession Codes

CCDC 2060640 and 2191096–2191099 contain the supplementary crystallographic data for this paper. These data can be obtained free of charge via www.ccdc.cam.ac.uk/data_request/cif, or by emailing data_request@ccdc.cam.ac.uk, or by contacting The Cambridge Crystallographic Data Centre, 12 Union Road, Cambridge CB2 1EZ, UK; fax: +44 1223 336033.

Complete contact information is available at: https://pubs.acs.org/10.1021/jacs.2c07726

The authors declare no competing financial interest.

Department of Chemistry and Biochemistry, Oberlin College, Oberlin, Ohio 44074, United States

M. Kevin Brown

Department of Chemistry, Indiana University, Bloomington, Indiana 47405, United States

Abstract

Photochemical dearomative cycloaddition has emerged as a useful strategy to rapidly generate molecular complexity. Within this context, stereo- and regiocontrolled intermolecular *para*-cycloadditions are rare. Herein, a method to achieve photochemical cycloaddition of quinolines and alkenes is shown. Emphasis is placed on generating sterically congested products and reaction of highly substituted alkenes and allenes. In addition, the mechanistic details of the process are studied, which revealed a reversible radical addition and a selectivity-determining radical recombination. The regio- and stereochemical outcome of the reaction is also rationalized.

Graphical Abstract

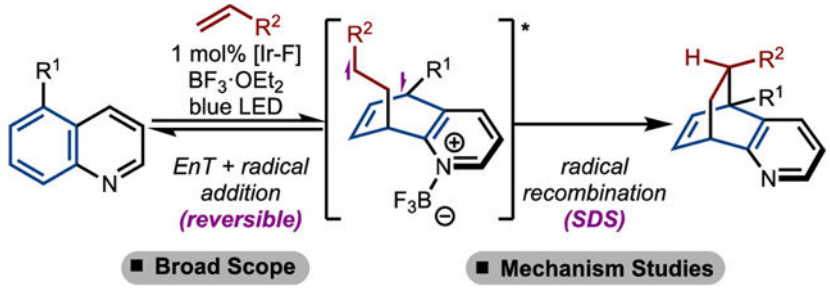

INTRODUCTION

Cycloaddition reactions are among the most efficient and atom-economical approaches to quickly build up molecular complexity.[1] Arene–alkene cycloaddition (AAC) reactions represent an ideal means of converting planar arenes into three-dimensional architectures.[2] However, most thermally induced dearomative cycloadditions are difficult to realize experimentally due to high kinetic barriers and competing reverse processes. Photochemically driven processes have allowed for the development of AAC as a photon allows for the reaction to proceed via excited-state intermediates.[3]

Photochemical cycloadditions between arenes and unsaturated systems (typically alkenes and acetylenes) can lead to the formation of *ortho, meta*, and *para* regioisomeric products (Scheme 1A).[4] Under direct irradiation, the singlet S_1 excited state of the arene is generated, and the formation of *meta*-cycloadducts dominates via a concerted cycloaddition.[5] However, if the triplet T_1 excited state is generated, arenes can behave more like diradicals, allowing access to *ortho* and *para* adducts via stepwise radical cycloaddition. Computational studies by Houk established this general paradigm,[6] which was further confirmed by Cornelisse and co-workers.[7] As the S_1 excited state of the arene can be easily accessed with simple UV-light irradiation, *meta* cycloadditions have been extensively studied and applied in the synthesis of various natural products.[3b,8,9]

Efficient access to the T_1 state of the arene through direct excitation is challenging for several reasons. First, the gap between S_0 and S_1 can be large, especially for S_1 ($\pi-\pi^*$).[10] As a result, short-wavelength irradiation with Hg lamps is usually required. Second, the transition from S_1 to T_1 may be difficult because of the relatively fast relaxation of S_1 to the ground state. Third, in accordance with El-Sayed's rule, a forbidden ISC would be necessary for the conversion of S_1 ($\pi-\pi^*$) to T_1 ($\pi-\pi^*$).[11] Finally, since *meta* cycloaddition can easily proceed via the S_1 state, there will likely be a competition among multiple cycloaddition pathways even if the T_1 state can be accessed. Despite these challenges, several *ortho*- and *para*-cycloadditions have been developed. For example, ortho-cycloadditions have been reported for systems in which the ISC to the T_1 ($\pi-\pi^*$) is facile. However, these systems are limited to specialized substrates with tethered alkenes.[12] Recently, developments have been made with phenanthrene derivatives in an intramolecular cycloaddition.[13] Only a few examples showed that electron-poor naphthalene derivatives could react with electron-deficient alkenes to yield the *para* cycloadducts.[14]

An alternative method to access the T_1 state of the arene is by visible-light mediated triplet–triplet energy transfer (EnT).[15] Because the T_1 state is accessed directly without having to generate S_1, only stepwise *ortho*-and *para*-cycloadditions are observed. Examples of EnT-induced dearomative *ortho*-cycloadditions include reactions of indoles[16] as reported by You,[17] Oderinde,[18] Fu,[19] and Zhang.[20] In addition, early work from Meggers demonstrated the dearomatization of benzofuran and benzothiophene.[21] Oderinde and co-workers later applied this strategy to electron-deficient indoles, benzofurans, benzothiophenes, and azaindoles.[22] Glorius also realized the *ortho* cycloaddition of benzothiophene via an endergonic EnT.[23] *para*-Cycloaddition is still rare under EnT conditions and mainly focuses on the sensitization of alkenes instead of arenes.[24]

Recently, our groups developed a selective intermolecular *para*-cycloaddition of bicyclic azaarenes with various activated and unactivated alkenes initiated by EnT (Scheme 1B).[25] This reaction displays good selectivity toward the formation of one isomer and affords valuable functionalized aromatic heterocycles that have been established as privileged motifs in pharmaceutically active compounds.[26] Additional studies revealed a novel photochemical cascade with certain substitution patterns.[27] In this study, we greatly expand upon the substrate scope to more challenging examples such as disubstituted alkenes and allenes under Lewis acid-mediated conditions developed in the Brown lab (Scheme 1C). In addition, we demonstrate that targets containing tetrasubstituted carbons can be accessed readily using this protocol. Finally, through a combination of mechanistic experiments and density functional theory (DFT) calculations, we present a detailed analysis of the reaction mechanism and reveal the energy landscape of the transformation.

RESULTS AND DISCUSSION

Initially, we employed 2-*i*Pr-thioxanthone (ITX, E_T = 65.4 kcal/mol)[28] as the photosensitizer for the reaction between quinoline (E_T = 61.9 kcal/mol) and 1-hexene, which resulted in <2% conversion. A similar result was obtained with $[Ir(dFCF_3ppy)_2dtbbpy]PF_6$ (Ir–F, E_T = 60.1 kcal/mol). Addition of 25 mol % $HNTf_2$ resulted in the formation of the *para* cycloadducts **2** and **3**, albeit in low yields (Table 1, entry 3). Further studies showed that

Lewis acids were more effective (Table 1, entries 4–5). We found that 125 mol % $BF_3{\cdot}OEt_2$ was required for full conversion (Table 1, entry 6), likely due to product inhibition. Finally, while the higher-energy sensitizer ITX gave a similar result as $[Ir(dFCF_3ppy)_2dtbbpy]PF_6$ (Table 1, entry 7), the use of lower-energy sensitizers led to diminished yields.

While evaluation of various Lewis acids, photosensitizers, and temperatures did not alter the selectivities, regioselectivity was found to be controlled by the polarity of the solvent and the position of the quinoline substituent (Scheme 2A). For these reactions, we define **2** as the 8-to-5 product and **3** as the 5-to-8 product based on the order of bond formation (*vide infra*). For quinoline (**1**), the 8-to-5 product **2** was the major regioisomer formed in all solvents evaluated, with the highest regioselectivity observed in toluene (12:1 rr). When 6-Me-quinoline was evaluated, a switch in regioselectivity occurred, yielding the 5-to-8 product as the major isomer. In addition, a similar correlation between regioselectivity and solvent polarity was observed, with MeCN yielding the highest regioselectivity for the 5-to-8 product (>20:1 rr).[29]

To understand the impact of substituent position on regioselectivity, we tested quinolines with methyl groups at different positions (Scheme 2B).[30,31] For quinolines with substitution on the pyridine ring (products **2**, **4**–**7**) or substitution on the 5- and 7-positions of the phenyl ring (products **8**–**9**), the 8-to-5 product was favored. The 5-to-8 product was preferentially formed when the substituent was in the 6- or 8-position on the phenyl ring (products **10**–**11**). A lower yield was found for formation of **5** and **11**, as coordination of the Lewis acid was likely impeded (see **12**). X-ray structures of **13** and **14** were obtained to confirm the identity of the major regioisomer.

We explored the reaction scope for 5-substituted quinolines due to both the high diastereo- and regioselectivities observed and the potential for constructing products containing sterically congested carbons (Scheme 3). Substituents with a wide range of steric and electronic properties were well-tolerated under the conditions. Various quaternary carbons were achieved with different sp^3 (products **8**, **15**–**16**, **19**) or sp^2 (products **17**–**18**) substituted quinolines. Heteroatom substituted centers with F (product **22**), Cl (product **23**), O (product **20**), N (product **21**), and Si (product **24**) were also easily prepared in high yields and selectivities. It is notable that intermolecular cycloaddition is faster than an intramolecular process (products **25**–**26**). This is likely due to the slow reaction between C8 and the terminal carbon of the alkene via an 8- or 9-membered transition state. The alkene scope was also broad with excellent functional group compatibility with alkenes (product **27**), ethers (product **30**), esters (product **29**), and halides (product **28**). All *mono*-substituted alkenes, regardless if activated (products **34**–**40**) or unactivated (products **27**–**33**), favored formation of the *endo*-diastereomer (dr ~ 10:1). Exclusive endo products (dr > 20:1) were found using styrenes regardless of the different substitution patterns. Even sterically demanding alkenes allowed for formation of the *endo*-products **31**–**33**. With 1,2-disubstituted alkenes, stereo-convergence to the *trans* product was observed from either *cis* or *trans* alkene inputs (product **42**–**43**), with the alkene substituent closer to the 5-position still being placed *endo* to the pyridine ring. Even for *cis*-cyclic alkenes like *cis*-cyclohexene, *cis*-cycloheptene, and *cis*-cyclooctene, the *trans* products **44**–**46** were isolated with high diastereoselectivity. The *anti*-structures **41**·MeI, **44**·MeI, and **46**·MeI were confirmed by X-ray analysis. The product

of *cis*-cyclooctadiene **47** was formed with lower dr, presumably because bond rotation was constrained by the internal alkene. For indene and dihydronaphthalene, bond rotation was even more constrained, and only the *cis-exo*-isomers were isolated (**49** and **50**). With respect to limitations, 1,1-di, tri-, and tetrasubstituted alkenes did not allow for product formation (products **51**–**52**). Finally, the reaction could be easily scaled up to 1.2 mmol/h using a flow chemistry system (**8**).

In addition to alkenes, allenes also underwent cycloadditions smoothly with quinoline substrates under standard conditions (Scheme 4, products **53**–**58**).[32] Regardless of the allene substitution pattern, the 8-to-5 product was exclusively formed. In the case of nonsymmetric allenes, mixtures of alkene isomers were formed (**54** and **56**). With 1,3-disubstituted allenes or trisubstituted allenes, the diastereoselectivities varied from *endo*- to *exo*-selective (products **56**–**58**).

Based on our previous report,[25] the mechanism of the reaction likely involves triplet–triplet energy transfer to a Lewis acid-activated quinoline followed by stepwise radical cycloaddition. However, there are several aspects that need to be considered in more detail (Scheme 5): (1) the role of the Lewis acid; (2) aromatic ring selectivity (benzene vs pyridine); (3) *ortho, meta*, and *para* selectivity; (4) 5-to-8 vs 8-to-5 regioselectivity; and (5) diastereoselectivity. We conducted further mechanistic studies to address all of these issues.

We first focused on determining the first nonreversible step of the reaction as it is important for understanding the origins of the observed selectivities.[33,34] To probe this, we conducted the standard reaction with the *E*-^{2}D-labeled alkene **59**. If the intermolecular radical addition step was selectivity-determining, we would expect to isolate **60a** and/or **60b** with recovered unchanged **59** (Scheme 6A). However, while **60a** and **60b** were isolated in a 1:1 mixture, the excess unreacted alkene **59** was recovered as a 1:1 mixture of *E*- and *Z*-isomers. One interpretation of this result is if the first intermolecular radical addition step is reversible and the second intramolecular radical recombination step is selectivity-determining. However, the isomerization of **59** could arise by an alternative unknown pathway. Therefore, ^{13}C kinetic isotope effects (KIEs) at natural abundance were determined using the methods developed by Singleton and co-workers (Scheme 6B).[35] We initially carried out KIE measurements on 5-Me-quinoline, the standard substrate in all DFT calculations, and observed a strong KIE at C5 (1.017). However, overlapping signals in the ^{13}C NMR spectra with C8 and C10 made it difficult to confirm the KIE value at C8. Thus, 5-OAc-quinoline was investigated and a similarly strong KIE at C5 was observed (1.019).

These mechanistic experiments strongly point to the first step being reversible and the intramolecular radical recombination being the selectivity-determining step. The observation that even *cis*-cyclic alkenes like cyclohexene preferentially form the *trans* product lends further support to the existence of a long-lived biradical intermediate that allows for bond rotation before recombination (see product **44**, Scheme 3). A revised mechanism is therefore proposed in Scheme 6C. Photo-sensitization of the BF_3 complex ^{1}**A** by the excited triplet state of [Ir–F] generates ^{3}**A**. Radical addition to 1-hexene then results in the formation of ^{3}**B**, which upon intersystem crossing yields the singlet ^{1}**B**. This singlet intermediate can

then undergo either radical fragmentation to revert to starting materials **^{1}A** and 1-hexene or recombination to yield product **^{3}C**.

To further reveal the energetic landscape traversed by the reaction, which our experiments suggested was more complex than previously assumed,[25,38] we performed DFT calculations (Scheme 6D). The three energy surfaces, triplet (T), open-shell singlet (OSS), and closed-shell singlet (CSS), were mapped out in detail along the reaction coordinates. At the beginning of the reaction, energy transfer from the excited photosensitizer to the ground-state quinoline–BF_3 **^{1}A** yields the triplet **^{3}A**. As the energy transfer process itself is not expected to impact the observed selectivities, we elected to focus our computational efforts on the subsequent transformations of **^{3}A**. Its reaction with propene (**60**) (used as a truncated computational model for 1-hexene) via **^{3}TS-1** on the triplet surface forms the first C–C bond with a calculated activation free energy of 15.6 kcal/mol. While the formation of the triplet biradical intermediate **^{3}B** is slightly exergonic, our calculations showed that it would most likely undergo intersystem crossing (ISC) to the open-shell singlet **^{1}B**, which lies about 4–6 kcal/mol below **^{3}B**. The OSS and CSS surfaces intersect at two transition points (**TPs**) where the open-shell and closed-shell wave functions transition smoothly: **TP-A**, which leads back to separated reactants, and **TP-B**, which furnishes the cycloadduct. Instead of being determined by only a single triplet radical addition transition state (**TS**), the chemo- and diastereoselectivities of the reaction are therefore controlled by the rate of ISC from **^{3}B** to **^{1}B**, as well as the energies of the OSS to CSS **TPs**.[36]

Two possible roles were hypothesized for the requirement of Lewis acid complexation in this reaction: (1) facilitating energy transfer by lowering E_T, and (2) accelerating the radical addition step by increasing the electrophilicity of the quinoline substrate. To probe the role of the Lewis acid in the energy transfer process,[37] we performed Stern–Volmer quenching studies. It was found that quinoline and quinoline–BF_3 complexes have similar quenching efficiencies (Scheme 7A). This result suggests that, while facilitating energy transfer, Lewis acid coordination is not strictly required for sensitization to happen. During the course of our study, Morofuji and Kano also showed that direct energy transfer to quinoline is feasible without the addition of an acid.[38,39] In contrast, the idea that Lewis acid primarily assists in the radical addition step found experimental support. When the standard reaction was conducted with *E*-^{2}D-labeled alkene **59** in the absence of BF_3, we observed <2% yield of the product and no epimerization of the alkene starting material, which indicated that the radical addition barrier was significantly higher without the Lewis acid (Scheme 7B).

To further verify that Lewis and/or Brønsted acid complexation has the effect of lowering the radical addition barriers, we calculated the radical addition **TSs** between various quinoline substrates and alkene partners. In all cases, the calculations confirmed that both Lewis and Brønsted acid complexation led to lower activation free energies ($\Delta G^{\ddagger}$) for the radical addition step (Scheme 7C). The magnitude of this effect is dependent on the identity of the acid as well as the quinoline/alkene combination, ranging from a 1.1 kcal/mol decrease for 5-Me-quinoline/propene (with BF_3 complexation) to 5.3 kcal/mol for the 3-Me-quinoline/2-butene (with H^+ complexation) system investigated by Morofuji and Kano.[38]

Equipped with a deeper understanding of the reaction mechanism, we next sought to rationalize the observed selectivities. Our calculations of the triplet-state quinoline substrates indicate that there is a higher spin density on the benzene moiety than the pyridine moiety with or without Lewis acid complexation (Figure 1), which is likely linked to the experimentally observed regioselectivity for the benzene ring.

We next turned our attention to rationalizing the observed *para* selectivity of the reaction over *ortho* (*meta* cycloadditions were not considered here as they are concerted and occur exclusively on the singlet energy surface). As our mechanistic studies revealed that the OSS to CSS **TPs** were likely the selectivity-determining structures in the reaction, we concentrated our efforts on locating and comparing the **TPs** for the *para* and *ortho* addition pathways. Because free energies cannot be calculated for these **TPs** as thermal contributions to energy from molecular vibrations cannot be obtained for nonstationary points on the potential energy surface,[39] we present the electronic energies in Scheme 8A for the *ortho*- and *para*-additions originating from ^{3}**B**. We found that for both the **TP** and the final cycloadduct, the calculated electronic energies of *ortho* were much higher (9 kcal/mol) than *para*. This result suggests that the formation of the *para* cycloadduct is likely kinetically favorable for this substrate.

Furthermore, the *ortho* and *para* products also differ in their photostability under the reaction conditions. The E_T of the *ortho* product ^{1}**D** was calculated to be 57.7 kcal/mol, which is smaller than that of the photosensitizer [Ir–F] (60.1 kcal/mol). In contrast, the *para* product ^{1}**C** had a calculated E_T of 76.5 kcal/mol, meaning that it is likely photostable under the reaction conditions. We therefore reasoned that the *ortho* product can be sensitized and undergo radical fragmentation back to the starting materials, which funnels the reaction toward exclusive *para* product formation.

Although we were not able to isolate an *ortho* product and confirm the photosensitization-induced fragmentation, we observed two fused-ring products, which may suggest that an *ortho* cycloaddition does occur under the reaction conditions for certain substitution patterns (Scheme 8B).[40] Cyclopropyl chloride **66** was isolated together with the *para* cycloadduct **67**. The formation of **66** can be rationalized through a second energy transfer to the *ortho* cycloadduct **62**, followed by C–Cl bond homolysis.[41] The resulting diradical **64** undergoes recombination to deliver **65**. In addition, in the case of **68**, a second energy transfer can occur to fragment the central C–C bond. Subsequent recombination can then yield a new cyclobutane product **73**. Overall, while formation of the para adducts is likely kinetically favored, for some substitution patterns, a photolabile *ortho*-adduct may be generated.

The 5-to-8 vs 8-to-5 regioselectivity of the reaction is also worthy of discussion. Having established through our mechanistic studies that the radical addition step is not selectivity-determining, we reasoned that the relative stability of the long-lived biradical intermediates could be key to explaining the regioselectivity. In the solvent-controlled regime (Scheme 2A), the biradical intermediate leading to the 5-to-8 product is expected to have a larger net dipole moment due to the alignment of partial dipoles (Scheme 9A). As a result, the 5-to-8 biradical intermediate would be better stabilized by more polar solvents. Our calculated dipole moment values (p_{calc}) for the biradical intermediates confirmed that the

5-to-8 biradical intermediate is more polar at 8.2 Debye, compared to 7.0 Debye for the 8-to-5 biradical intermediate. This is in good agreement with our experimental observations that higher-polarity solvents favor the 5-to-8 product.

In the substitution-controlled regime (Scheme 2B), the stability of the biradical intermediates is primarily dictated by the degree of hyperconjugation. In these cases, the formation of the more stable biradical may render it less likely to undergo fragmentation back to starting materials. With an alkyl substituent in the 5- or 7-position, the biradical intermediate leading to the 8-to-5 product is better stabilized by hyper-conjugative donation than its 5-to-8 counterpart (Scheme 9B). This explains the preferential formation of the 8-to-5 product for the 5- and 7-substituted substrates. For quinoline substrates with substitution in the 6- or 8-position, the 5-to-8 biradical intermediate would be better stabilized by hyperconjugation, leading to the opposite regioselectivity.

Finally, we set out to rationalize the *endo* diastereoselectivity of the reaction, for which we proposed that London dispersion forces could be the key factor (Scheme 10).[42] To verify that dispersive interactions favor the formation of the *endo* product diastereomer, we compared **TP** energies calculated at the B3LYP/def2-TZVPP, SMD(CH_2Cl_2) (not dispersion-corrected), and B3LYP-D3/def2-TZVPP, SMD(CH_2Cl_2) (dispersion-corrected) levels (Scheme 10B). Our results confirmed that the electronic energies of the **TPs** leading to the *endo* diastereomers are indeed lowered more compared to the *exo* diastereomers when a dispersion-corrected functional was applied. In the reaction between 5-Me-quinoline and propene, dispersion correction favors the *endo*-product-forming **TP** by 0.7 kcal/mol relative to its *exo* counterpart. When the alkene substituent is a larger *tert*-butyl group instead of the methyl group of propene, this effect is even more pronounced, with dispersion adding 1.8 kcal/mol favorability to the *endo*-product-forming **TP**. Noncovalent interaction (NCI) plots for the MECPs also showed that at these C–C-forming bond lengths, the alkene substituent is within the right distance range to have favorable dispersive interactions with the pyridine moiety of the quinoline when in the *endo* position. These computational results showed that dispersion indeed has the effect of steering diastereoselectivity toward the *endo* product isomer.

CONCLUSIONS

We described herein a dearomative *para* -cycloaddition of quinolines with a variety of activated and unactivated alkenes. The reaction was enabled by photosensitization of the Lewis acid-complexed substrates and displays high diastereo- and regioselectivities that are tunable through varying the solvent and substitution patterns. Our mechanistic studies revealed a complex multisurface energetic landscape traversed by the reaction. Using a combined experimental and computational approach, we also disclosed the origins of the observed regio- and diastereoselectivities. Given the emerging interest in bridged polycycles and heterocycles in medicinal chemistry, we anticipate that this method will find substantial use in facilitating the efficient synthesis of such scaffolds.

Supplementary Material

Refer to Web version on PubMed Central for supplementary material.

ACKNOWLEDGMENTS

The authors thank Indiana University and the NIH (R35GM131755) for financial support. This project was partially funded by the Vice Provost for Research through the Research Equipment Fund and the NSF MRI programs, CHE-1726633 and CHE-1920026. Support for the acquisition of the Bruker Venture D8 diffractometer through the Major Scientific Research Equipment Fund from the President of Indiana University and the Office of the Vice President for Research is gratefully acknowledged. S.C. is grateful to Oberlin College for financial support. DFT calculations were performed using the SCIURus, the Oberlin College HPC cluster (NSF MRI 1427949). Generous financial support by the University of Munster and the Deutsche Forschungsgemeinschaft (SFB 858) is gratefully acknowledged.

REFERENCES

(1). (a)Carruthers W; Baldwin JECycloaddition Reactions in Organic Synthesis, Elsevier Science, 1990.(b)Kobayashi S; Jørgensen KACycloaddition Reactions in Organic Synthesis; Wiley-VCH Verlag GmbH: Weinheim, Germany, 2001.(c)Nishiwaki NMethods and Applications of Cycloaddition Reactions in Organic Syntheses; John Wiley & Sons: New York, 2014.

(2). (a)Ritchie TJ; Macdonald SJF The impact of aromatic ring count on compound developability – are too many aromatic rings a liability in drug design? Drug Discovery 2009, 14, 1011–1020. (b)Lovering F; Bikker J; Humblet C Escape from Flatland: Increasing Saturation as an Approach to Improving Clinical Success. J. Med. Chem 2009, 52, 6752–6756. [PubMed: 19827778] (c)Lovering F Escape from Flatland 2: complexity and promiscuity. Med. Chem. Commun 2013, 4, 515–519.(d)Mykhailiuk PK Saturated bioisosteres of benzene: where to go next? Org. Biomol. Chem 2019, 17, 2839–2849. [PubMed: 30672560] (e)Subbaiah MAM; Meanwell NA Bioisosteres of the Phenyl Ring: Recent Strategic Applications in Lead Optimization and Drug Design. J. Med. Chem 2021, 64, 14046–14128. [PubMed: 34591488]

(3). For selected reviews see: (a)Streit U; Bochet CG The Arene-Alkene Photocycloaddition. Beilstein J. Org. Chem 2011, 7, 525–542. [PubMed: 21647263] (b)Remy R; Bochet CG Arene–Alkene Cycloaddition. Chem. Rev 2016, 116, 9816–9849. [PubMed: 27340900] (c)Okumura M; Sarlah D Visible-Light-Induced Dearomatizations. Eur. J. Org. Chem 2020, 2020, 1259–1273.(d)Cheng Y-Z; Feng Z; Zhang X; You S-L Visible-Light Induced Dearomatization Reactions. Chem. Soc. Rev 2022, 51, 2145–2170. [PubMed: 35212320]

(4). Gilbert A The Inter- and Intramolecular Photocycloaddition of Ethylenes to Aromatic Compounds. Pure Appl. Chem 1980, 52, 2669–2682.

(5). Bryce-Smith D Orbital Symmetry Relationships for Thermal and Photochemical Concerted Cycloadditions to the Benzene Ring. J. Chem. Soc. D 1969, 806–808.

(6). Houk KN Theory of Cycloadditions of Excited Aromatics to Alkenes. Pure Appl. Chem 1982, 54, 1633–1650.

(7). van der Hart JA; Mulder JJC; Cornelisse J Funnels and barriers in the photocycloaddition of arenes to alkenes and dienes. J. Photochem. Photobiol. A 1995, 86, 141–148.

(8). Cornelisse J The Meta Photocycloaddition of Arenes to Alkenes. Chem. Rev 1993, 93, 615–669.

(9). (a)Wender PA; Ternansky R; deLong M; Singh S; Olivero A; Rice K Arene-Alkene Cycloadditions and Organic Synthesis. Pure Appl. Chem 1990, 62, 1597–1602.(b)Kärkäs MD; Porco JA; Stephenson CRJJ Photochemical Approaches to Complex Chemotypes: Applications in Natural Product Synthesis. Chem. Rev 2016, 116, 9683–9747. [PubMed: 27120289]

(10). Anslyn EV; Dougherty DAModern Physical Organic Chemistry; University Science Books: Sausalito, CA, 2006; Chapter 16, pp 935–1000.

(11). El-Sayed MA The Triplet State: Its Radiative and Nonradiative Properties. Acc. Chem. Res 1968, 1, 8–16.

(12). Wagner PJ Photoinduced Ortho [2 + 2] Cycloaddition of Double Bonds to Triplet Benzenes. Acc. Chem. Res 2001, 34, 1–8. [PubMed: 11170351]

(13). (a)Mattay J Selectivities in Photocycloadditions of Arenes to Olefins. J. Photochem 1987, 37, 167–183.(b)Stegbauer S; Jandl C; Bach T Enantioselective Lewis Acid Catalyzed *ortho* Photocycloaddition of Olefins to Phenanthrene-9-carboxaldehydes. Angew. Chem., Int. Ed 2018, 57, 14593–14596.

(14). (a)Döpp D; Krüger C; Memarian HR; Tsay Y-H 1,4-Photocycloaddition of *α*-Morpholinoacrylonitrile to 1-Acylnaphthalenes. Angew. Chem., Int. Ed 1985, 24, 1048–1049. (b)Ohkura K; Sugaoi T; Sakushima A; Nishijima K; Kuge Y; Seki K Thermodynamically Controlled Photocycloaddition of 5-Fluoro-1,3-dimethyluracil to Naphthalenes. Heterocycles 2002, 58, 595–600.

(15). For selected reviews, see: (a)Strieth-Kalthoff F; James MJ; Teders M; Pitzer L; Glorius F Energy transfer catalysis mediated by visible light: principles, applications, directions. Chem. Soc. Rev 2018, 47, 7190–7202. [PubMed: 30088504] (b)Zhou Q-Q; Zou Y-Q; Lu L-Q; Xiao W-J Visible-Light-Induced Organic Photochemical Reactions through Energy-Transfer Pathways. Angew. Chem., Int. Ed 2019, 58, 1586–1604.(c)Strieth-Kalthoff F; Glorius F Triplet Energy Transfer Photocatalysis: Unlocking the Next Level. Chem 2020, 6, 1888–1903.(d)Großkopf J; Kratz T; Rigotti T; Bach T Enantioselective Photochemical Reactions Enabled by Triplet Energy Transfer. Chem. Rev 2022, 122, 1626–1653. [PubMed: 34227803]

(16). Ma J; Schäfers F; Daniliuc C; Bergander K; Strassert CA; Glorius F Gadolinium Photocatalysis: Dearomative [2 + 2] Cycloaddition/Ring-Expansion Sequence with Indoles. Angew. Chem., Int. Ed 2020, 59, 9639–9645.

(17). (a)Zhu M; Zheng C; Zhang X; You S-L Synthesis of Cyclobutane-Fused Angular Tetracyclic Spiroindolines Via Visible-Light-Promoted Intramolecular Dearomatization of Indole Derivatives. J. Am. Chem. Soc 2019, 141, 2636–2644. [PubMed: 30653315] (b)Zhu M; Huang X-L; Xu H; Zhang X; Zheng C; You S-L Visible-Light-Mediated Synthesis of Cyclobutene-Fused Indolizidines and Related Structural Analogs. CCS Chem. 2020, 2, 652–664.(c)Zhu M; Zhang X; Zheng C; You S-L Visible-Light-Induced Dearomatization via [2+2] Cycloaddition or 1,5-Hydrogen Atom Transfer: Divergent Reaction Pathways of Transient Diradicals. ACS Catal. 2020, 10, 12618–12626.(d)Zhu M; Huang X-L; Sun S; Zheng C; You S-L Visible-Light-Induced Dearomatization of Indoles/Pyrroles with Vinylcyclopropanes: Expedient Synthesis of Structurally Diverse Polycyclic Indo-lines/Pyrrolines. J. Am. Chem. Soc 2021, 143, 13441–13449. [PubMed: 34398603]

(18). Oderinde MS; Mao E; Ramirez A; Pawluczyk J; Jorge C; Cornelius LAM; Kempson J; Vetrichelvan M; Pitchai M; Gupta A; Gupta AK; Meanwell NA; Mathur A; Dhar TGM Synthesis of Cyclobutane-Fused Tetracyclic Scaffolds via Visible-Light Photo-catalysis for Building Molecular Complexity. J. Am. Chem. Soc 2020, 142, 3094–3103. [PubMed: 31927959]

(19). Zhang Z; Yi D; Zhang M; Wei J; Lu J; Yang L; Wang J; Hao N; Pan X; Zhang S; Wei S; Fu Q Photocatalytic Intramolecular [2 + 2] Cycloaddition of Indole Derivatives via Energy Transfer: A Method for Late-Stage Skeletal Transformation. ACS Catal. 2020, 10, 10149–10156.

(20). Zhuang W; Cheng Y-Z; Huang X-L; Huang Q; Zhang X Visible-Light Induced Divergent Dearomatization of Indole Derivatives: Controlled Access to Cyclobutane-Fused Polycycles and 2-Substituted Indolines. Org. Chem. Front 2021, 8, 319–325.

(21). Hu N; Jung H; Zheng Y; Lee J; Zhang L; Ullah Z; Xie X; Harms K; Baik M-H; Meggers E Catalytic Asymmetric Dearomatization by Visible-Light-Activated [2 + 2] Photocycloaddition. Angew. Chem., Int. Ed 2018, 57, 6242–6246.

(22). Oderinde MS; Ramirez A; Dhar TGM; Cornelius LAM; Jorge C; Aulakh D; Sandhu B; Pawluczyk J; Sarjeant AA; Meanwell NA; Mathur A; Kempson J Photocatalytic Dearomative Intermolecular [2 + 2] Cycloaddition of Heterocycles for Building Molecular Complexity. J. Org. Chem 2021, 86, 1730–1747. [PubMed: 33356273]

(23). Strieth-Kalthoff F; Henkel C; Teders M; Kahnt A; Knolle W; Gómez-Suárez A; Dirian K; Alex W; Bergander K; Daniliuc CG; Abel B; Guldi DM; Glorius F Discovery of Unforeseen Energy-Transfer-Based Transformations Using a Combined Screening Approach. Chem 2019, 5, 2183–2194.

(24). (a)Kishikawa K; Akimoto S; Kohmoto S; Yamamoto M; Yamada K Intramolecular photo[4+2]cycloaddition of an enone with a benzene ring. J. Chem. Soc., Perkin Trans 1 1997, 77–84.(b)Ma J; Strieth-Kalthoff F; Dalton T; Freitag M; Schwarz JL; Bergander K; Daniliuc C;

Glorius F Direct Dearomatization of Pyridines via an Energy-Transfer-Catalyzed Intramolecular [4 + 2] Cycloaddition. Chem 2019, 5, 2854–2864.

(25). Ma J; Chen S; Bellotti P; Guo R; Schafer F; Heusler A; Zhang X; Daniliuc C; Brown MK; Houk KN; Glorius F Photochemical intermolecular dearomative cycloaddition of bicyclic azaarenes with alkenes. Science 2021, 371, 1338–1345. [PubMed: 33766881]

(26). (a)Taylor RD; MacCoss M; Lawson AD Rings in Drugs. J. Med. Chem 2014, 57, 5845–5859. [PubMed: 24471928] (b)Vitaku E; Smith DT; Njardarson JT Analysis of the Structural Diversity, Substitution Patterns, and Frequency of Nitrogen Heterocycles among U.S. FDA Approved Pharmaceuticals. J. Med. Chem 2014, 57, 10257–10274. [PubMed: 25255204] (c)Blakemore DC; Castro L; Churcher I; Rees DC; Thomas AW; Wilson DM; Wood A Organic Synthesis Provides Opportunities to Transform Drug Discovery. Nat. Chem 2018, 10, 383–394. [PubMed: 29568051]

(27). (a)Ma J; Chen S; Bellotti P; Wagener T; Daniliuc C; Houk KN; Glorius F Facile access to fused 2D/3D rings via intermolecular cascade dearomative [2 + 2] cycloaddition/rearrangement reactions of quinolines with alkenes. Nat. Catal 2022, 5, 405–413.(b)Bellotti P; Rogge T; Paulus F; Laskar R; Rendel N; Ma J; Houk KN; Glorius F Visible-Light Photocatalyzed *peri*-(3 + 2) Cycloadditions of Quinolines. J. Am. Chem. Soc 2022, 144, 15662–15671. [PubMed: 35984989]

(28). Elliott LD; Kayal S; George MW; Booker-Milburn K Rational Design of Triplet Sensitizers for the Transfer of Excited State Photochemistry from UV to Visible. J. Am. Chem. Soc 2020, 142, 14947–14956. [PubMed: 32786778]

(29). Reichardt C; Welton TSolvents and Solvent Effects in Organic Chemistry, 3rd ed.; Wiley-VCH Publishers, 2003; pp 470–475.

(30). During the investigation we found it necessary to switch from the optimized solvent PhMe to CH_2Cl_2, and to dilute the reaction to [0.05 M] for improved solubility (especially for substituted quinolines).[22]

(31). Chénard E; Sutrisno A; Zhu L; Assary RS; Kowalski JA; Barton JL; Bertke JA; Gray DL; Brushett FR; Curtiss LA; Moore JS Synthesis of Pyridine– and Pyrazine–BF_3 Complexes and Their Characterization in Solution and Solid State. J. Phys. Chem. C 2016, 120, 8461–8471.

(32). For photochemical reaction with allenes, see: (a)Haddaway K; Somekawa K; Fleming P; Tossell JA; Mariano PS Chemistry of Allene Cation Radicals Probed by the Use of Theoretical and Electron-transfer Photochemical Methods. J. Org. Chem 1987, 52, 4239–4253. (b)Birbaum F; Neels A; Bochet CG Photochemistry of Allenyl Salicylaldehydes. Org. Lett 2008, 10, 3175–3178. [PubMed: 18597474] (c)Streit U; Birbaum F; Quattropani A; Bochet CG Photocycloaddition of Arenes and Allenes. J. Org. Chem 2013, 78, 6890–6910. [PubMed: 23641810]

(33). Several previous studies have proposed that the first step is the selectivity determining step. See refs 19, 22, 23.

(34). For a recent study that highlights a selectivity determining radical recombination, see Zhu M; Zheng C Post-Spin Crossing Dynamics Determine the Regioselectivity in Open-Shell Singlet Biradical Recombination. Org. Chem. Front 2022, 9, 995–1003.

(35). (a)Singleton DA; Thomas AA High-Precision Simultaneous Determination of Multiple Small Kinetic Isotope Effects at Natural Abundance. J. Am. Chem. Soc 1995, 117, 9357–9358.(b)Beno BR; Houk KN; Singleton DA Synchronous or Asynchronous? An “Experimental” Transition State from a Direct Comparison of Experimental and Theoretical Kinetic Isotope Effects for a Diels–Alder Reaction. J. Am. Chem. Soc 1996, 118, 9984–9985.(c)Hirschi JS; Takeya T; Hang C; Singleton DA Transition State Geometry Measurements from ^{13}C Isotope Effects. The Experimental Transition State for the Epoxidation of Alkenes with Oxaziridines. J. Am. Chem. Soc 2009, 131, 2397–2403. [PubMed: 19146405] (d)For ^{13}C KIE at natural abundance to probe a photochemical reaction, see:[13] Kuan K-Y; Singleton DA Isotope Effects and the Mechanism of Photoredox-Promoted [2 + 2] Cycloadditions of Enones. J. Org. Chem 2021, 86, 6305–6313. [PubMed: 33890775]

(36). It is also possible that the trajectory of approach of the alkene to the triplet quinoline diradical may influence the selectivity.

(37). Daub ME; Jung H; Lee BJ; Won J; Baik M-H; Yoon TP Enantioselective [2+2] Cycloadditions of Cinnamate Esters: Generalizing Lewis Acid Catalysis of Triplet Energy Transfer. J. Am. Chem. Soc 2019, 141, 9543–9547. [PubMed: 31145856]

(38). Morofuji T; Nagai S; Chitose Y; Abe M; Kano N Protonation-Enhanced Reactivity of Triplet State in Dearomative Photocycloaddition of Quinolines to Olefins. Org. Lett 2021, 23, 6257–6261. [PubMed: 34324819] The free energy barriers shown in Scheme 7C were re-calculated and differ from those calculated by the original authors.

(39). Gaussian 16 Users Reference, Keyword: Freq, 2021. https://gaussian.com/man/.

(40). (a) see ref 27. (b)Zhu M; Xu H; Zhang X; Zheng C; You S-L Visible-Light-Induced Intramolecular Double Dearomative Cycloaddition of Arenes. Angew. Chem., Int. Ed 2021, 60, 7036–7040.

(41). For triplet radical H atom abstraction, see: (a) ref 27 (b)Xiong Y; Großkopf J; Jandl C; Bach T Visible Light-Mediated Dearomative Hydrogen Atom Abstraction/Cyclization Cascade of Indoles. Angew. Chem., Int. Ed 2022, 61, No. e202200555.

(42). For selected reviews, see: (a)Krenske EH; Houk KN Aromatic Interactions as Control Elements in Stereoselective Organic Reactions. Acc. Chem. Res 2013, 46, 979–989. [PubMed: 22827883] (b)Wagner JP; Schreiner PR London Dispersion in Molecular Chemistry-Reconsidering Steric Effects. Angew. Chem., Int. Ed 2015, 54, 12274–12296.(c)Wheeler SE; Seguin TJ; Guan Y; Doney AC Noncovalent Interactions in Organocatalysis and the Prospect of Computational Catalyst Design. Acc. Chem. Res 2016, 49, 1061–1069. [PubMed: 27110641] (d)Grimme S; Hansen A; Brandenburg JG; Bannwarth C Dispersion-Corrected Mean-Field Electronic Structure Methods. Chem. Rev 2016, 116, 5105–5154. [PubMed: 27077966] (e)Bursch M; Caldeweyher E; Hansen A; Neugebauer H; Ehlert S; Grimme S Understanding and Quantifying London Dispersion Effects in Organometallic Complexes. Acc. Chem. Res 2019, 52, 258–266. [PubMed: 30586286] (f)Pollice R; Chen P A Universal Quantitative Descriptor of the Dispersion Interaction Potential. Angew. Chem., Int. Ed 2019, 58, 9758–9769.

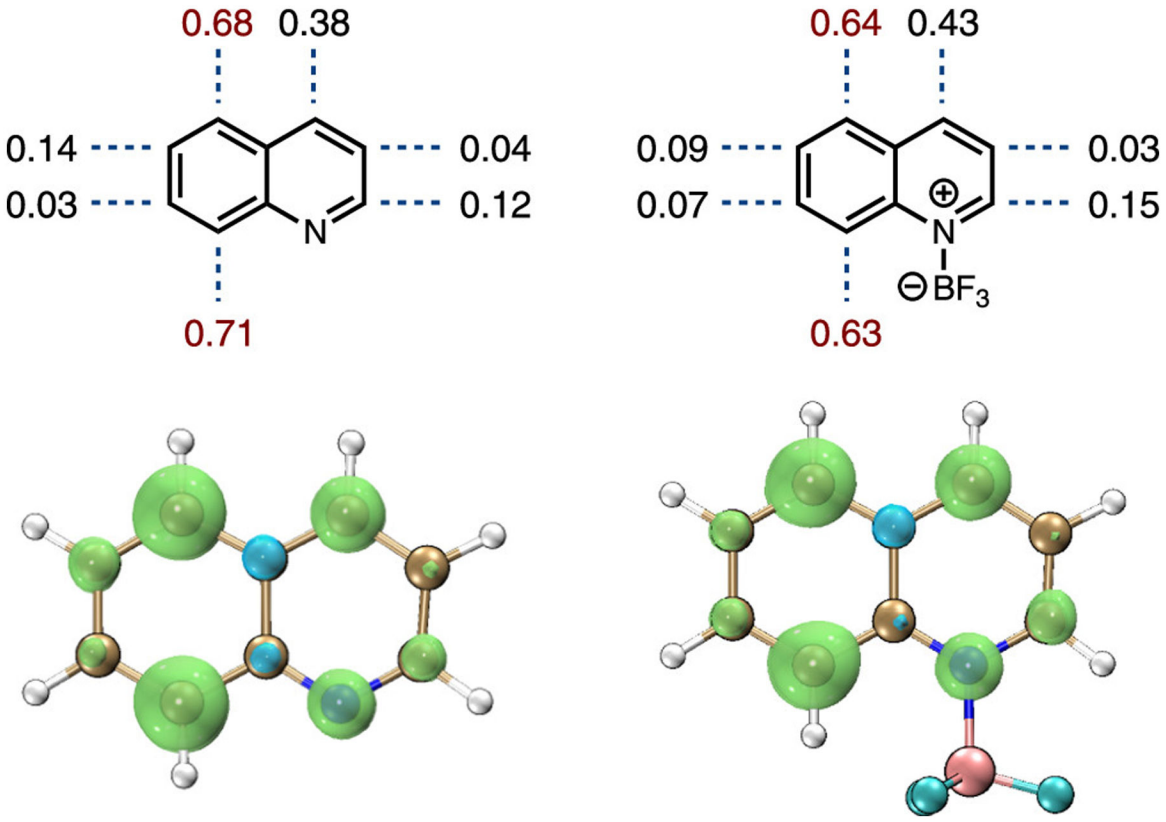

Figure 1.
Calculated spin densities.

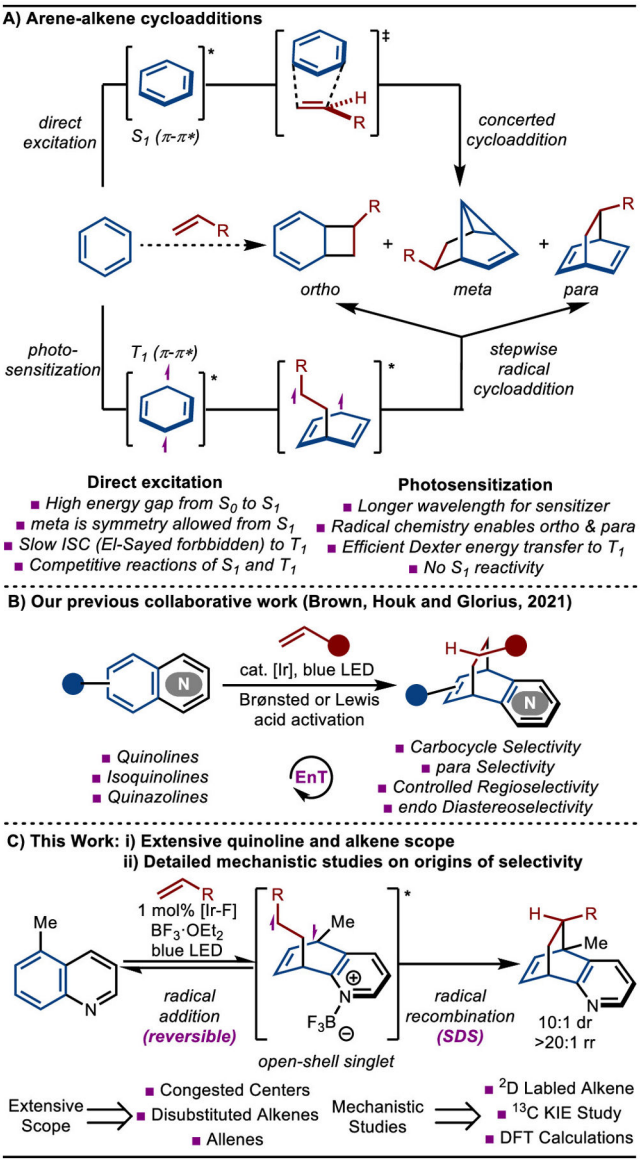

Scheme 1.
Arene–Alkene Cycloaddition

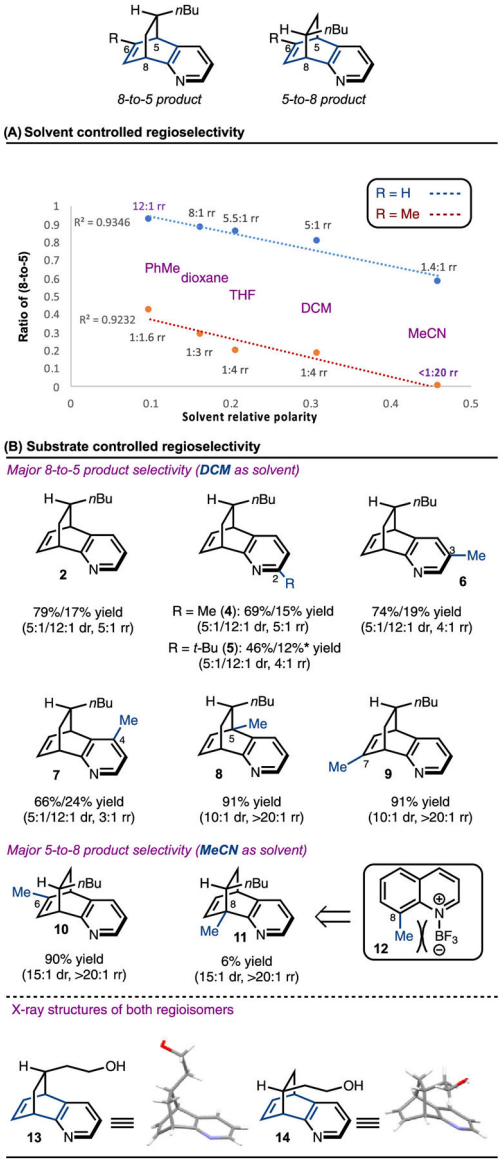

Scheme 2.

Regioselectivity[a]

[a]Reactions were run on a 0.25 mmol scale with standard conditions; yield of the isolated product is reported as combined yields of both diastereomers, average of two runs; dr and rr were determined by NMR analysis of the unpurified mixture. *NMR yield.

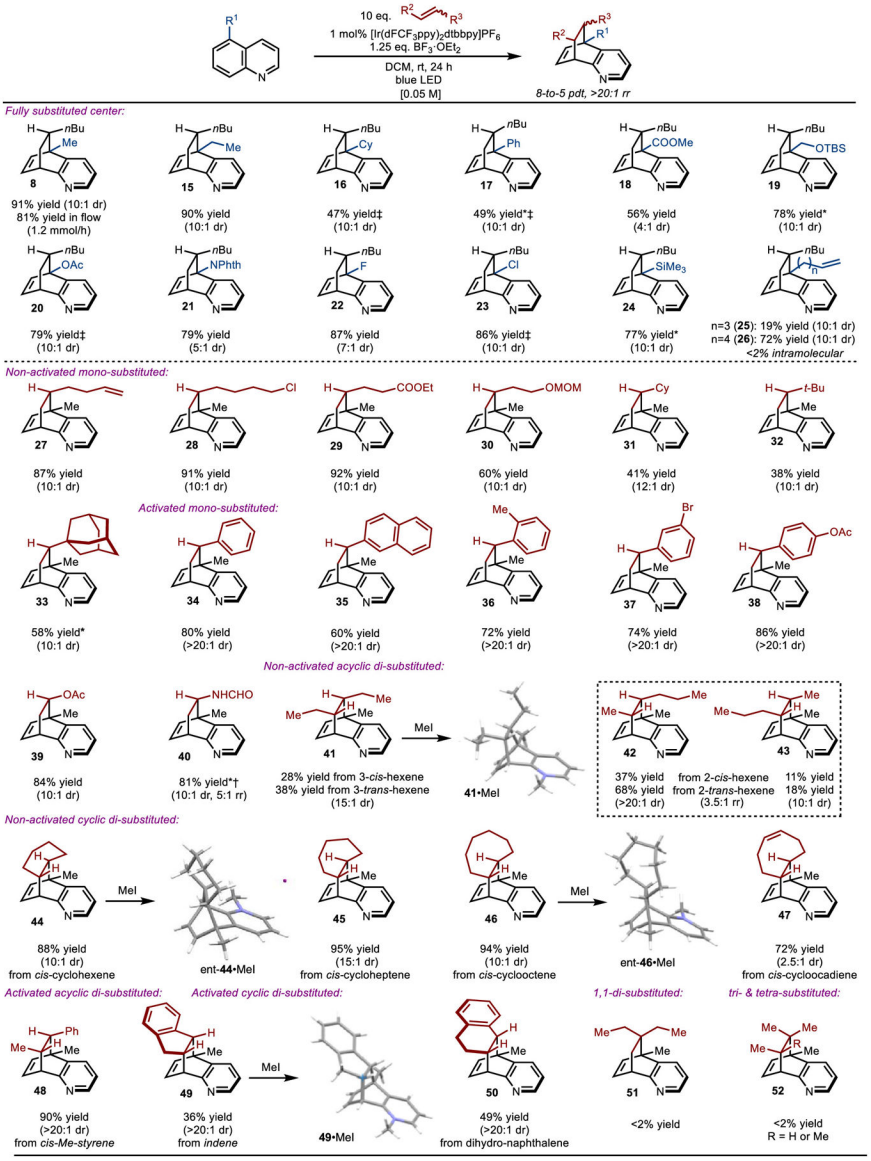

Scheme 3.

Substrate Scope[a]

[a]Reactions were run on a 0.25 mmol scale; yields of isolated products were reported as combined yields of both diastereomers; dr and rr were determined by NMR analysis of the unpurified mixture; average of two runs. Condition for methylation: MeI (5 equiv), dioxane, 50 °C, 12 h; *48 h; †yields of all for diastereo- and regioisomers; ‡>20:1 dr after purification.

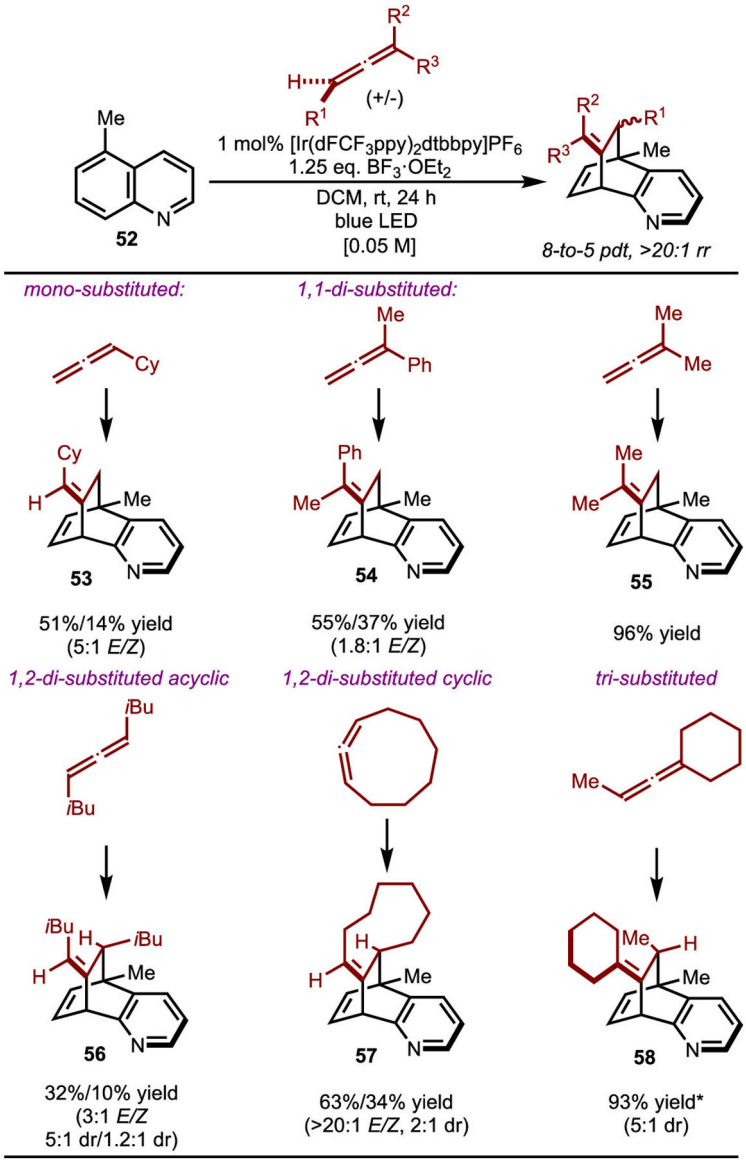

Scheme 4.

Allene Scope[a]

[a]Reactions were run on a 0.25 mmol scale; values of dr, rr, and *E*/*Z* were determined by NMR analysis of the unpurified reaction mixture. *Combined yield of both diastereomers. Average of two runs.

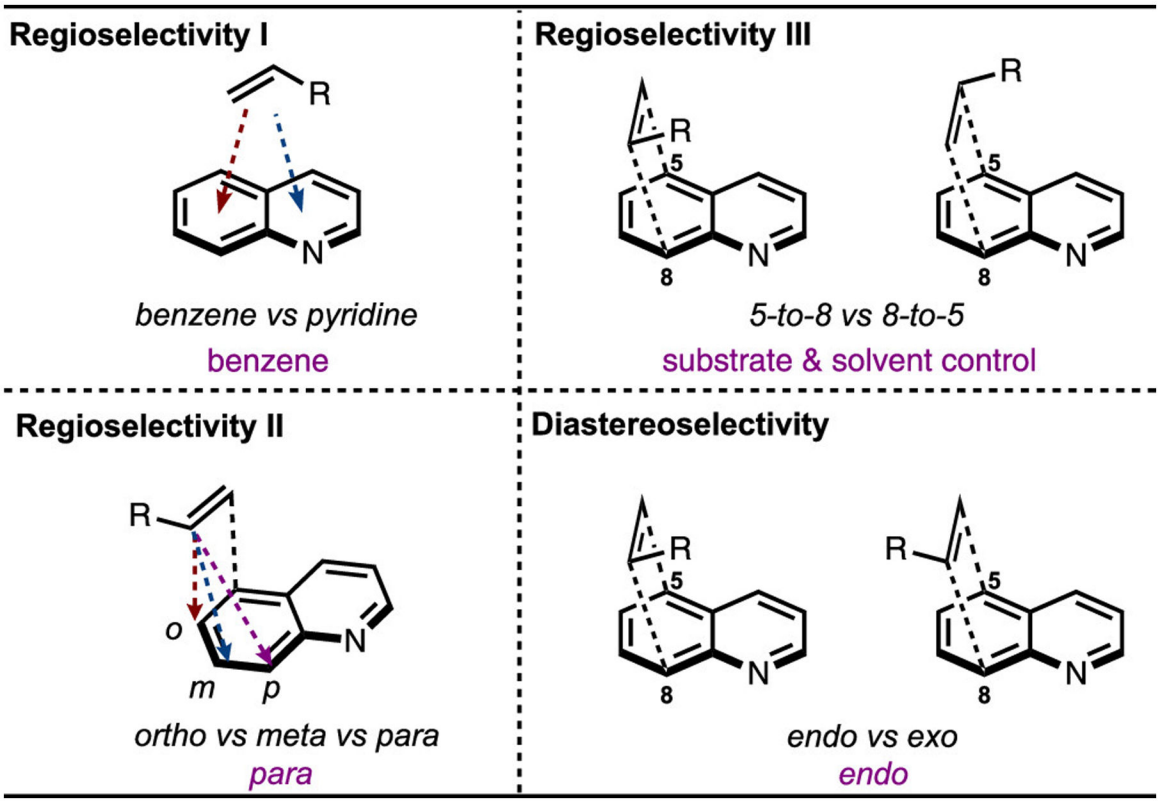

Scheme 5.
Selectivity Challenges

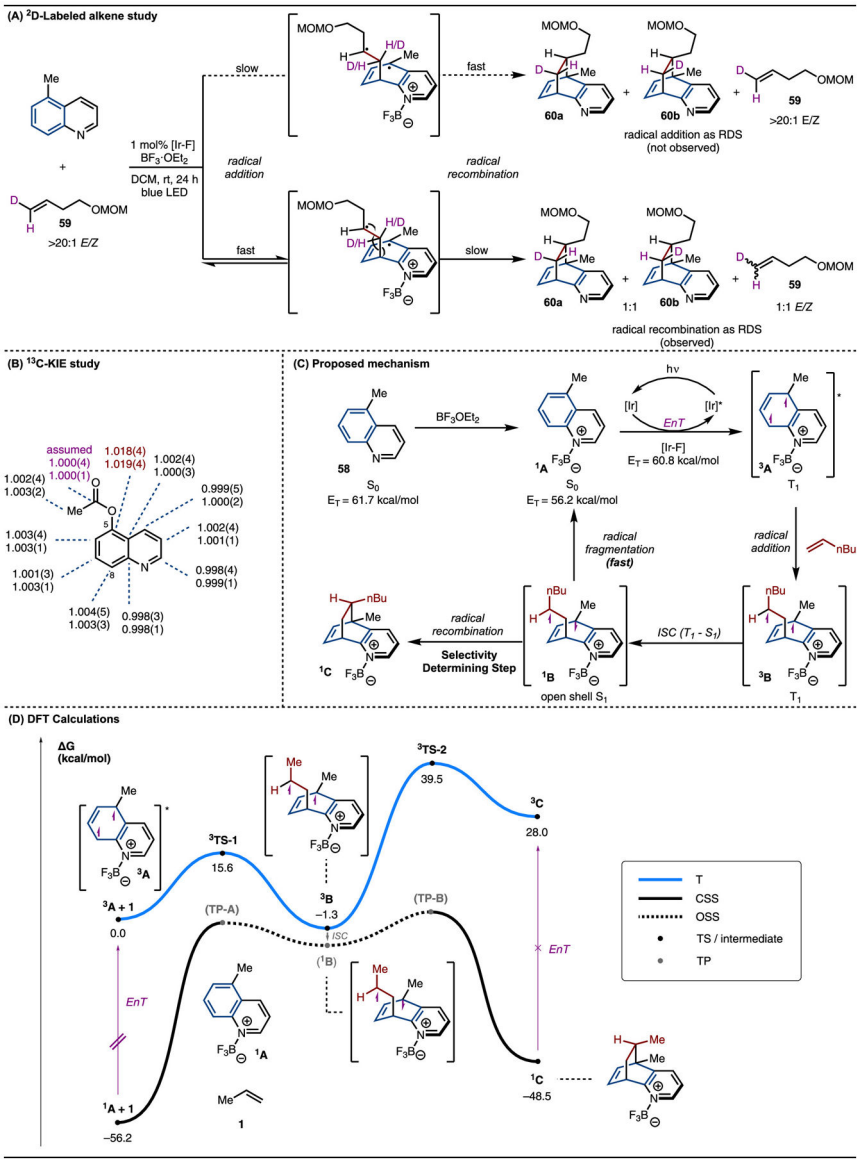

Scheme 6.
Selectivity-Determining Step

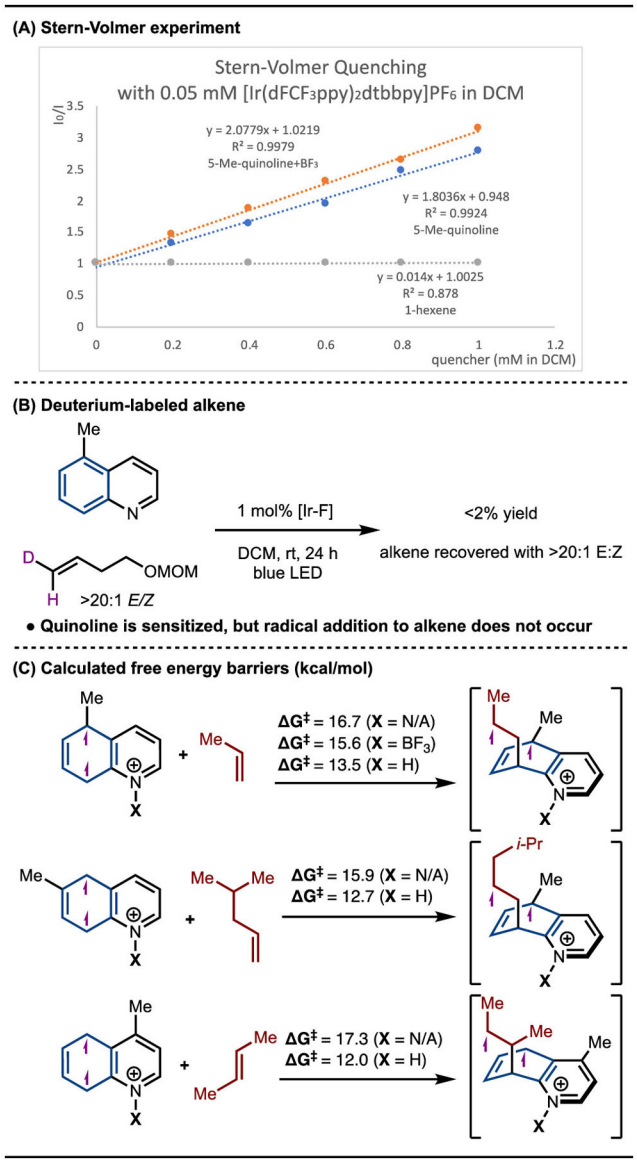

Scheme 7.
Role of Lewis Acid

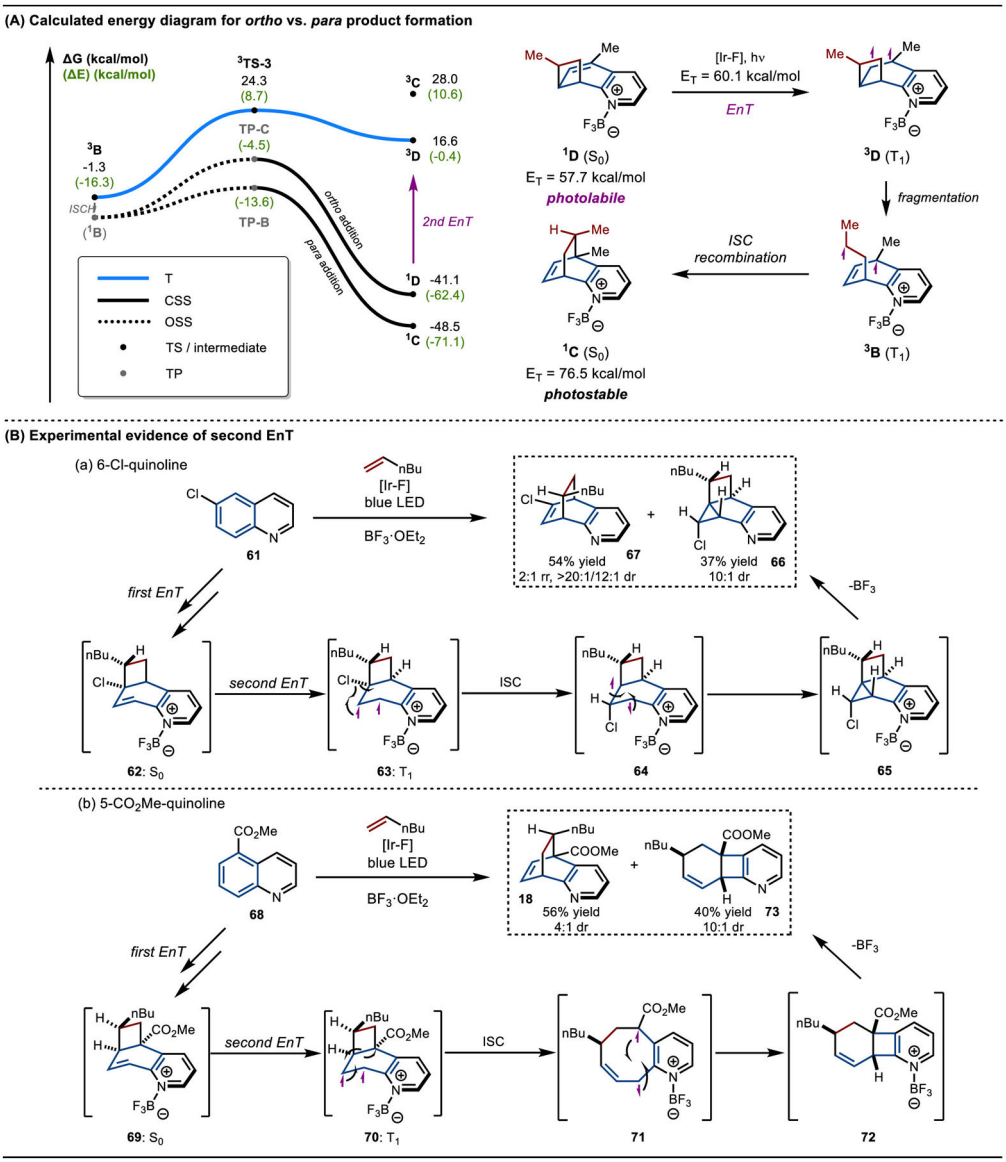

Scheme 8.

Ortho vs *Para* Selectivity

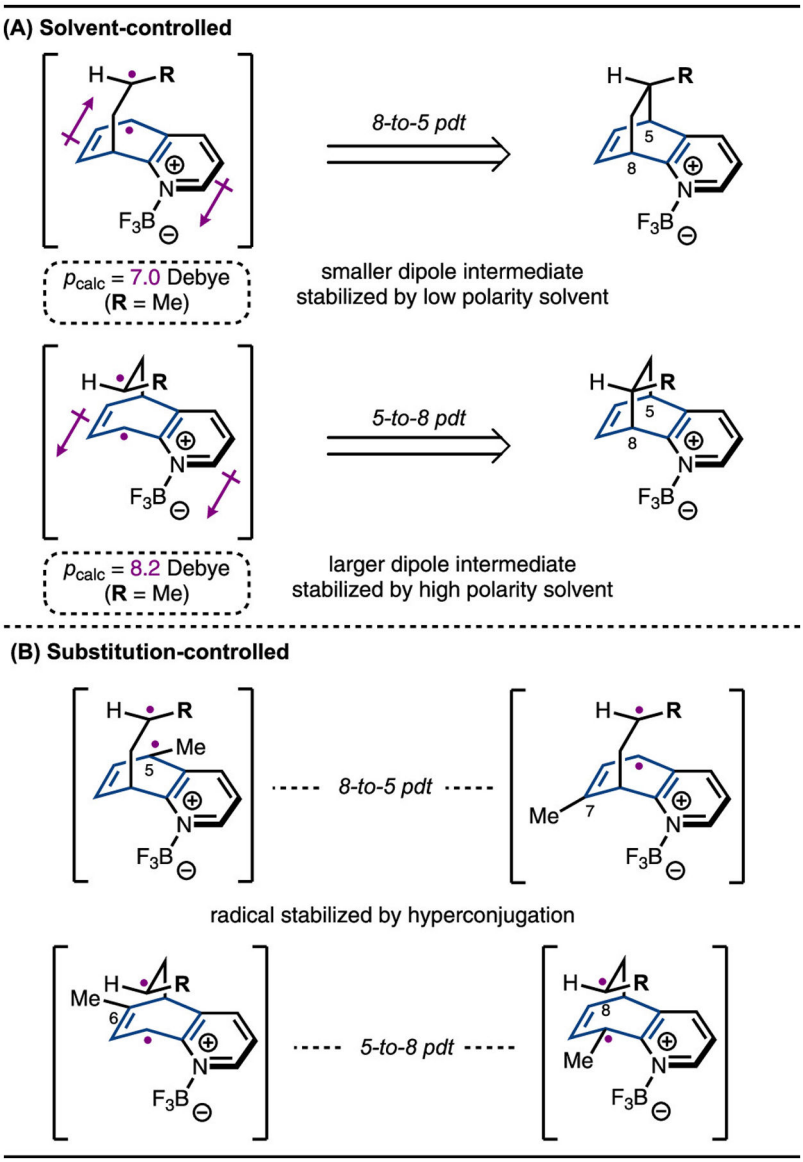

Scheme 9.

5-to-8 vs 8-to-5 Regioselectivity

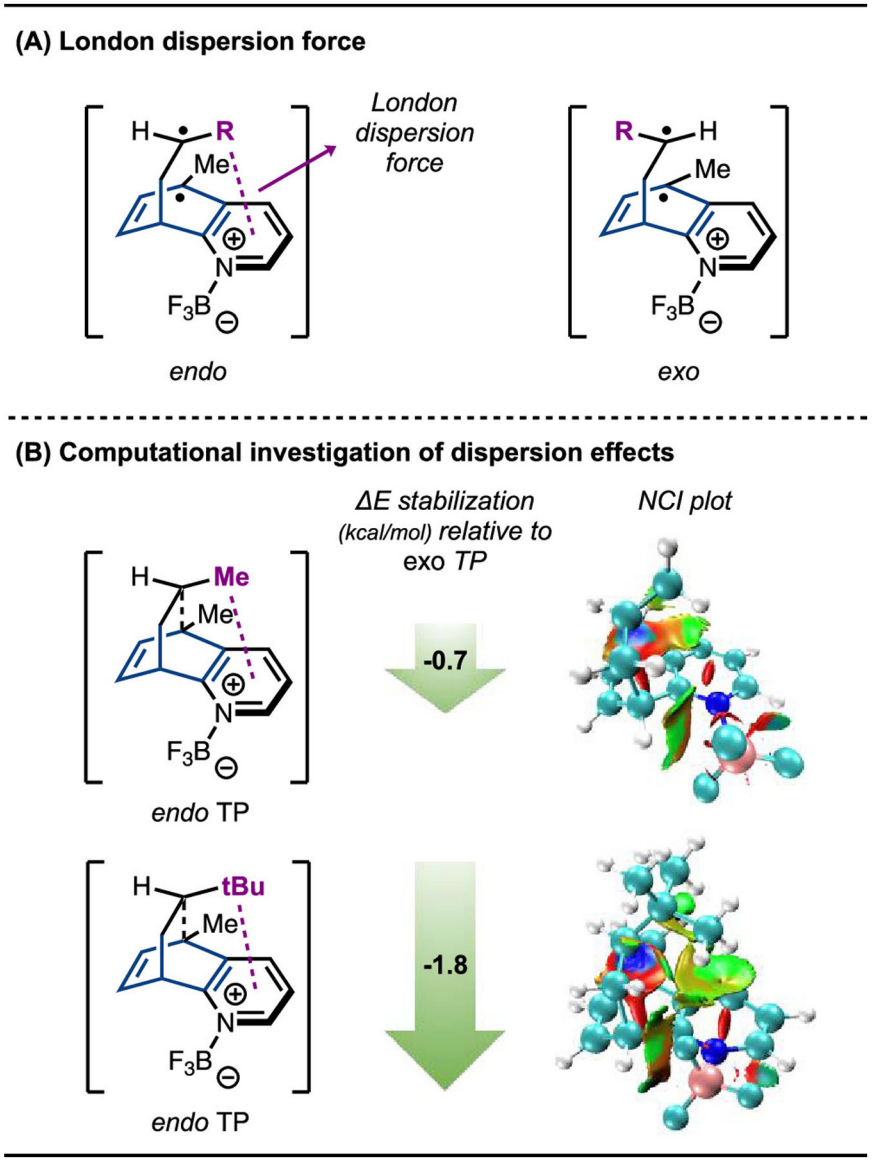

Scheme 10.
Endo vs *Exo* Diastereoselectivity

Table 1.

Reaction Optimization

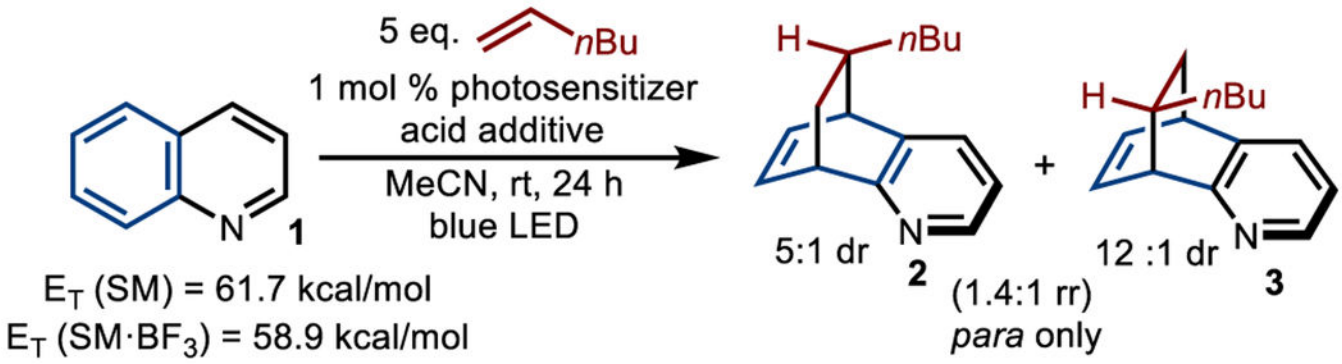

entry[a]	photosensitizer	E_T (kcal/mol)	acids	yield (%)[b]
1	2-*i*Pr-thioxanthone[c]	65.4	-	<2
2	$[Ir(dFCF_3ppy)_2dtbbpy]PF_6$	60.1	-	<2
3	$[Ir(dFCF_3ppy)_2dtbbpy]PF_6$	60.1	25 mol % $HNTf_2$	~10
4	$[Ir(dFCF_3ppy)_2dtbbpy]PF_6$	60.1	25 mol % $Sc(OTf)_3$	26
5	$[Ir(dFCF_3ppy)_2dtbbpy]PF_6$	60.1	25 mol % $BF_3{\cdot}OEt_2$	24
6	$[Ir(dFCF_3ppy)_2dtbbpy]PF_6$	60.1	125 mol % $BF_3{\cdot}OEt_2$	>95
7	2-*i*-Pr-thioxanthone[c]	65.4	125 mol % $BF_3{\cdot}OEt_2$	>95
8	$[Ir(dFppy)_2dtbbpy]PF_6$	57.1	125 mol % $BF_3{\cdot}OEt_2$	33
9	*fac*-$Ir(ppy)_3$	55.2	125 mol % $BF_3{\cdot}OEt_2$	<2

[a] Reactions were run on a 0.1 mmol scale.

[b] Combined yields (rr and dr) were determined by crude NMR for using CH_2Br_2 as the internal standard.

[c] 5 mol % cat., 395 nm LED, 36 h.